Multi-Hazards Susceptibility Assessment for Landslides and Floods in Hunza-Nagar, Northern Pakistan

Izhar Ahmad [1], Muhammad Ashraf [1], and Muhammad Waseem [1*]

[1] Department of Civil Engineering, Ghulam Ishaq Khan Institute of Engineering Sciences and Technology, Topi 23640, Pakistan
* Correspondence: muhammad.waseem@giki.edu.pk

Abstract

The destructive potential of natural hazards has increased due to rapid urbanization and greater exposure, leading to significant loss of life, infrastructure damage, and environmental degradation. Floods and landslides, among the most prevalent geo-hazards, often occur simultaneously in vulnerable regions. This study focuses on the hazard component of disaster risk by developing a multi-hazard susceptibility map (MHSM) for the Hunza-Nagar region, prone to both floods and landslides. For landslide susceptibility, the Frequency Ratio (FR) model is employed, considering geo-environmental factors like elevation, slope, LULC, rainfall, lithology, and proximity to roads, rivers, and faults. A landslide inventory of 139 events is split into training (70%) and validation (30%) datasets, achieving an accuracy of 91.6%. For flood susceptibility, the Random Forest (RF) model is applied using ten explanatory factors. A 100-year return period flood simulation in HEC-RAS provides flood extents from which flood inventory is prepared, achieving an accuracy of 91.2%. The MHSM integrates FR-based landslide and RF-based flood susceptibility maps using a combined sum approach in GIS. The region is classified into four zones: No Hazard, Flood Hazard, Landslide Hazard, and Combined Hazard. The MHSM maintains high prediction accuracy and serves as a reliable tool for identifying multi-hazard zones. This map is essential for disaster management authorities and infrastructure planners, enabling targeted mitigation strategies to reduce hazard impacts and enhance regional resilience.

Keywords: Multi-Hazard Susceptibility Map (MHSM); Floods and landslides; Hazard Zoning

1. Introduction

Natural hazards such as floods and landslides are among the most frequent and destructive events globally, posing substantial risks to populations, infrastructure, and the environment. These hazards rarely occur in isolation, particularly in mountainous regions, where the interplay between geological, climatic, and anthropogenic factors exacerbates risks [1], [2]. Climate change has intensified this issue, increasing the frequency and magnitude of extreme weather events, thereby amplifying the potential for cascading hazards [3]. The interconnected nature of floods and landslides, especially in fragile and complex topographical environments like the Hunza-Nagar Valley in northern Pakistan, highlights the need for an integrated and multi-hazard risk assessment framework.

Traditionally, hazard studies have focused on single events, such as floods or landslides, analyzed in isolation without considering their interrelated or cascading effects [4], [5]. However, in real-world scenarios, regions are often exposed to multiple hazards that may occur simultaneously or sequentially, triggering further disruptions [6]. For example,

intense monsoon rains combined with rapid snowmelt often lead to floods, which can destabilize slopes, resulting in landslides [7]. In mountainous terrains, glacial lake outburst floods (GLOFs) are particularly concerning due to their unpredictability and destructive capacity [8], [9]. Historical records indicate that the Hunza-Nagar Valley has experienced approximately 35 GLOF events in the past two centuries, with significant damage recorded in recent incidents, such as the 2018 Badswat GLOF and the 2022 Shisper GLOF [10]. Such events underscore the need for comprehensive flood and landslide susceptibility mapping to mitigate risks effectively.

The Sendai Framework for Disaster Risk Reduction emphasizes the importance of adopting integrated risk management strategies to build community resilience and reduce disaster impacts [11]. A multi-hazard approach provides a holistic framework by considering not only the spatial and temporal overlap of hazards but also their cumulative, synergistic, and cascading effects [12]. Unlike single-hazard models, multi-hazard assessments address the limitations of fragmented risk analyses, improving the accuracy of predictions and facilitating more effective mitigation planning. Additionally, incorporating socioeconomic factors such as population density, infrastructure vulnerability, and land use patterns enhances the understanding of human capacity and resilience.

Despite its advantages, implementing a multi-hazard susceptibility framework presents significant challenges. These include the lack of a universally accepted definition of multi-hazard risk, the integration of diverse hazard datasets, and the need for reliable geospatial data, particularly in remote and complex terrains [13]. However, advancements in remote sensing and geospatial technologies now provide critical tools for overcoming these barriers. Airborne remote sensing, for instance, offers valuable insights into hazard susceptibility across varying scales, aiding in the identification of vulnerable zones [14], [15].

The Hunza-Nagar Valley serves as a representative case study for multi-hazard assessment due to its susceptibility to both floods and landslides. The region's steep slopes, fragile geological formations, and exposure to extreme climatic events create a unique setting for studying hazard interdependencies [16]. During the summer monsoon season, heavy rainfall and melting alpine snow frequently saturate river catchments, causing floods that threaten human lives, infrastructure, and agricultural land [7]. Concurrently, unstable slopes in the region are prone to landslides, which further compound the risks and economic losses [17]. In light of the escalating frequency of such events, it is imperative to develop robust multi-hazard susceptibility maps that integrate flood and landslide risks to inform disaster management strategies.

This paper addresses the need for a comprehensive multi-hazard susceptibility assessment in the Hunza-Nagar Valley. By integrating machine learning and statistical techniques, the study aims to evaluate the region's vulnerability to floods and landslides, offering a critical tool for policymakers and disaster management agencies. The findings contribute to improving risk mitigation, supporting sustainable infrastructure development, and enhancing community resilience against future hazards.

2. Methodology

2.1. Study Area

The study area is located in the Hunza-Nagar region of Gilgit-Baltistan (GB), spanning 36° 51′ 34.40″ N to 35° 51′ 22.32″ N latitude and 76° 1′ 44.29″ E to 73° 58′ 27.43″ E longitude, with elevations ranging from 1,662 to 7,822 meters above sea level (Fig. 1). Covering 14,449 km², the region features a moderate climate, with temperatures ranging from 16°C to 35.9°C and an annual average precipitation of 136.2 mm, peaking in April (28.3 mm) and reaching its lowest in November (2.1 mm) [18].

Strategically important, the Karakoram Highway (KKH) passes through Hunza-Nagar, connecting China and Pakistan. However, the region is prone to geological hazards due to fractured geology, rugged terrain, and tectonic activity. The area comprises key lithological units: the Southern Karakoram Metamorphic Complex (SKM), the Chalt Group, and the Hunza Plutonic Unit (HPU), with lithology including gneiss, andesites, quartz, and unconsolidated mass. More than 70% of the valley lies on the Main Karakoram Thrust fault, making it susceptible to landslides [19]. Notably, the 2010 Attabad landslide led to the loss of lives, displacement of communities, and the submersion of 19 km of the KKH [20].

The Hunza River, fed by glacial melt and monsoonal rainfall, plays a vital role in local agriculture and hydrology but also increases flood vulnerability. The region faces multiple hazards, including riverine floods, urban flooding, and Glacial Lake Outburst Floods (GLOFs), such as the 2010 Attabad Lake incident [21]. Given these risks, flood susceptibility mapping is essential to protect communities and infrastructure from potential disasters.

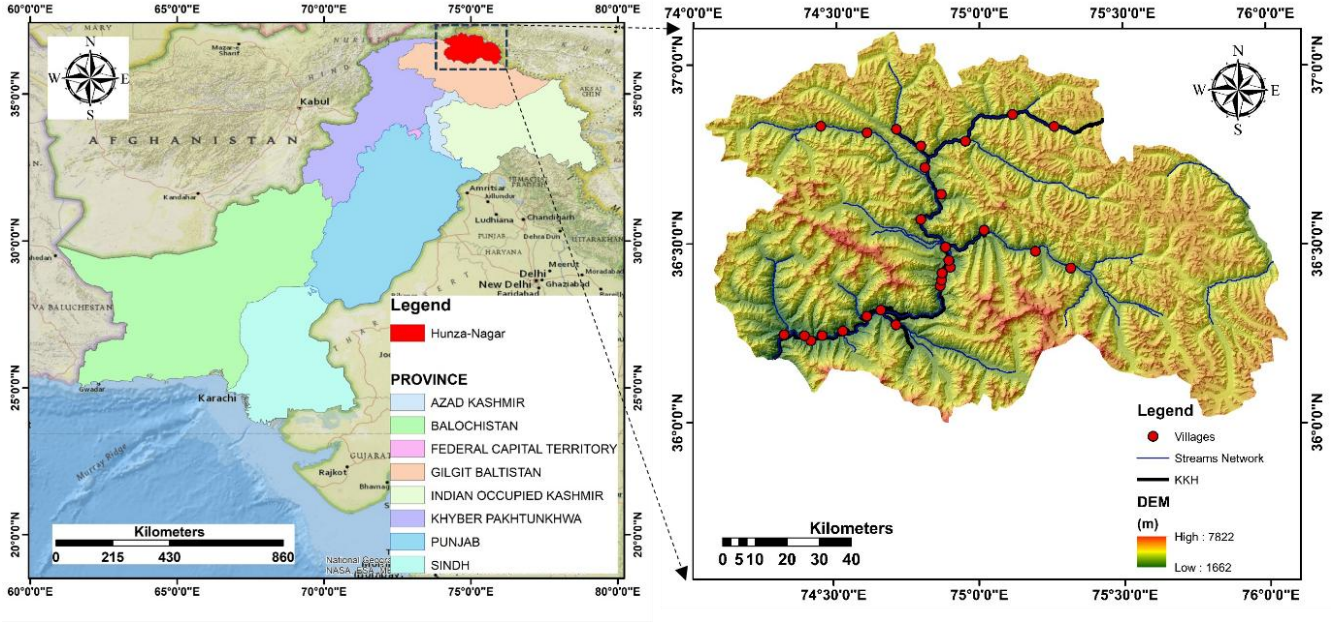

Figure 1. Geographic location of study area

2.2. Landslide Susceptibility Assessment

This study applies bi-variate statistical model to develop a Landslide Susceptibility Map (LSM) for the Hunza-Nagar Valley using remote sensing data and geospatial tools. The methodology includes compiling a landslide inventory, preprocessing causative factors from open-source remote sensing data, calculating factor weights using statistical technique, generating the LSM, and validating the model (see Fig. 2).

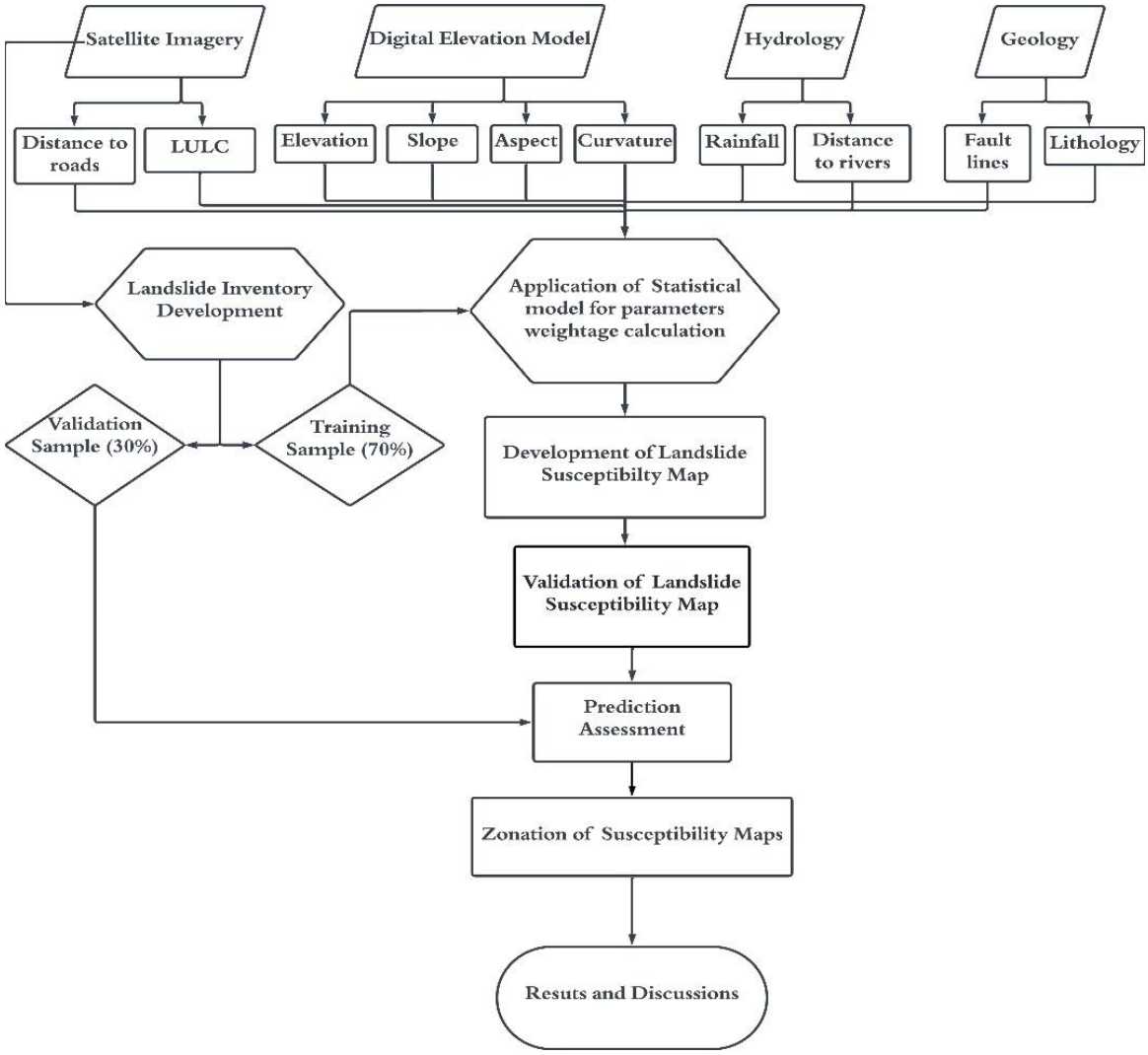

Figure 2. Methodology Flowchart for LSM.

2.2.1. Landslide Inventory

The landslide inventory maps historical landslides using satellite imagery, field surveys, and government records. In this study, 139 landslides of varying scales, including rockfalls, debris flows, and bank slides, were identified (Fig. 3). GPS coordinates and Google Earth Engine imagery were used to delineate landslide boundaries as polygons, which were rasterized in a GIS environment for statistical analysis. For model development, 70% of the inventory data was used for training, while 30% was reserved for validation and accuracy assessment.

2.2.2. Landslide Conditioning Factors

The landslide susceptibility analysis incorporates ten key factors influencing slope stability (see Fig. 3): elevation, which affects drainage patterns and precipitation distribution; slope, a critical factor as steep slopes increase shear stress and trigger downslope movements; curvature, which regulates water flow and influences gravitational forces on slopes; and aspect, which determines sunlight exposure, moisture retention, and vegetation cover impacting slope stability. Land Use/Land Cover (LULC) identifies varying impacts on slope stability, where vegetation enhances stability while barren land increases vulnerability. Rainfall significantly influences pore pressure and rock fracturing, serving as a primary landslide trigger. Lithology highlights the resistance of compact rocks versus the susceptibility of loose formations. Distance to roads reflects human interventions like

blasting and excavations that destabilize slopes. Distance to rivers captures the effects of erosion, infiltration, and saturation on slope bases, leading to failures. Lastly, distance to faults underscores geological instabilities caused by cracks, fissures, and tectonic activity, elevating landslide susceptibility.

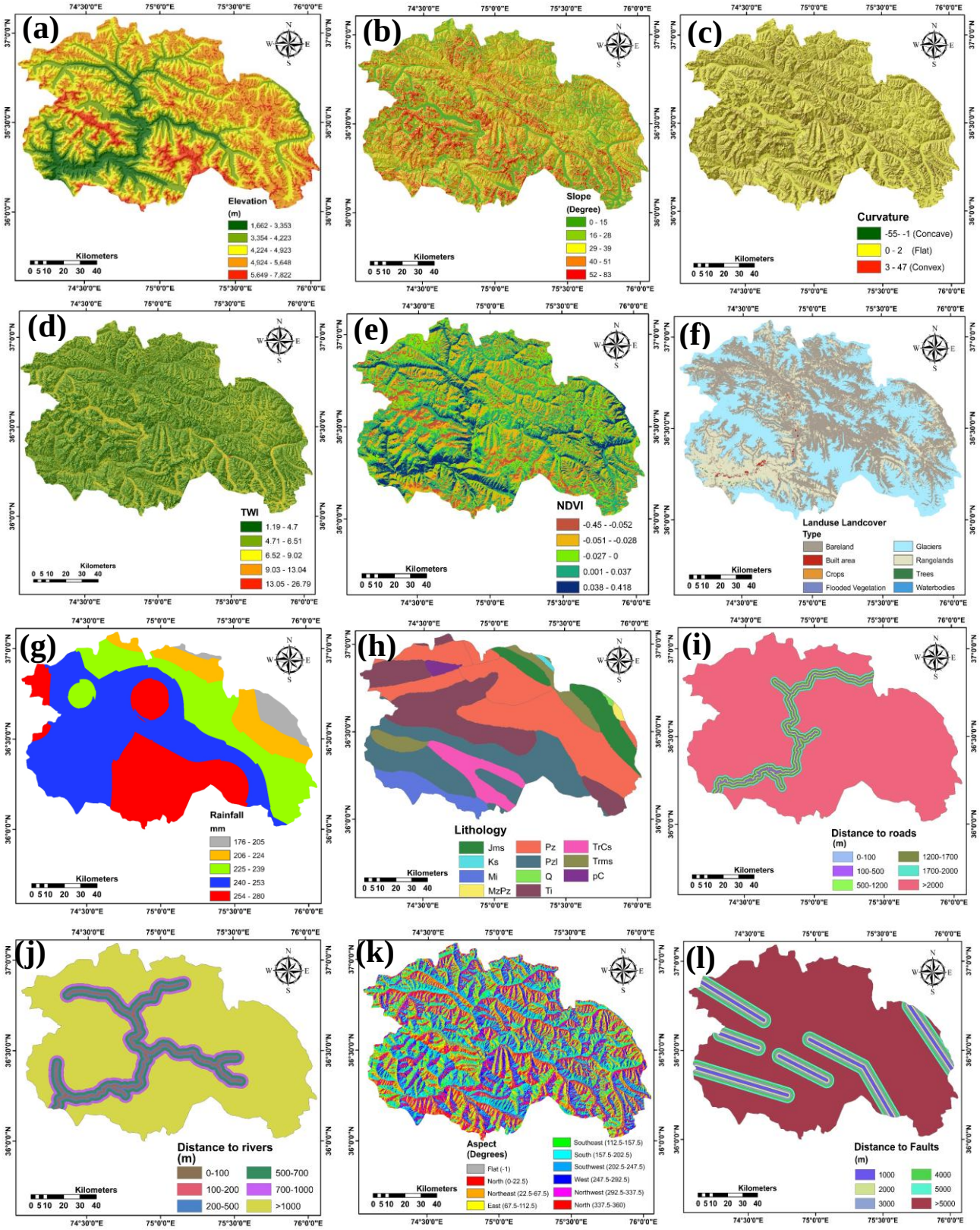

Figure 3. Conditioning factors for landslide and flood.

2.2.3. Frequency Ratio (FR)

FR statistical model is utilized in assessing the spatial correlation between regions affected by landslides and the factors contributing to their occurrence [22]. This method operates on a conditional probability model, facilitating a quantitative evaluation of the relationship between landslide incidents and diverse causal elements. By comparing the ratio of landslide-affected pixels to a given conditioning factor, a stronger association is indicated by a higher ratio, representing greater consideration in the formulation of Landslide Susceptibility Index (LSI) maps [23]. Implementing the FR model involves the consideration of each class of causal factors, juxtaposing landslide-affected and unaffected pixels for analysis. Equation 1 represents the statistical expression utilized to compute the FR weightage for each class of the causal factor, guiding the delineation of susceptibility patterns with greater precision and accuracy.

$$FR_i = \frac{N_{p(Si)} / N_{p(Ni)}}{\sum N_{p(Si)} / \sum N_{p(Ni)}} \quad (1)$$

Where $N_{p\,(Si)}$ = Count of landslides effected pixels in class i, $Np_{\,(Si)}$ = Total count of pixels in the same class i, $\Sigma\, N_{p\,(Si)}$ = Count of landslides effected pixels for all classes, $\Sigma\, N_{p\,(Si)}$ = Total count of pixels in all classes for the entire study area. The values obtained from equation 1 are utilized in equation 2 to obtain LSI map for the whole study area.

$$LSI = \sum_{i=1}^{n} FR_i \quad (2)$$

2.3. Flood Susceptibility Assessment

The methodology for developing flood susceptibility maps (FSMs) integrates ensemble machine learning technique with hydrodynamic modeling and satellite-derived data. The process involves selecting and processing flood conditioning factors, conducting unsteady flow simulations to create a flood inventory, applying machine learning algorithms to generate FSMs, evaluating model performance using accuracy metrics. A comprehensive flowchart illustrating this methodology is provided in Fig. 4.

2.3.1. Flood Inventory

A comprehensive flood inventory for the Hunza River was developed using the flood polygon generated from the spatial extent of a 100-year return period flood. The polygon, derived through 2D unsteady flow analysis in HEC-RAS 6.4.1, covers an area of 71.5 km² and was imported into ArcGIS 10.8.2. Within this inundated area, 1500 flood points were selected, and an equal number of non-flood points were randomly sampled outside the flood zone to ensure an unbiased dataset. These points were combined, with flood points labeled as 1 and non-flood points as 0, and split into training (70%) and testing (30%) datasets for machine learning algorithms. This approach surpasses traditional FSM methodologies by incorporating a 100-year return period flood, enabling predictions for more severe flood events under changing climate scenarios.

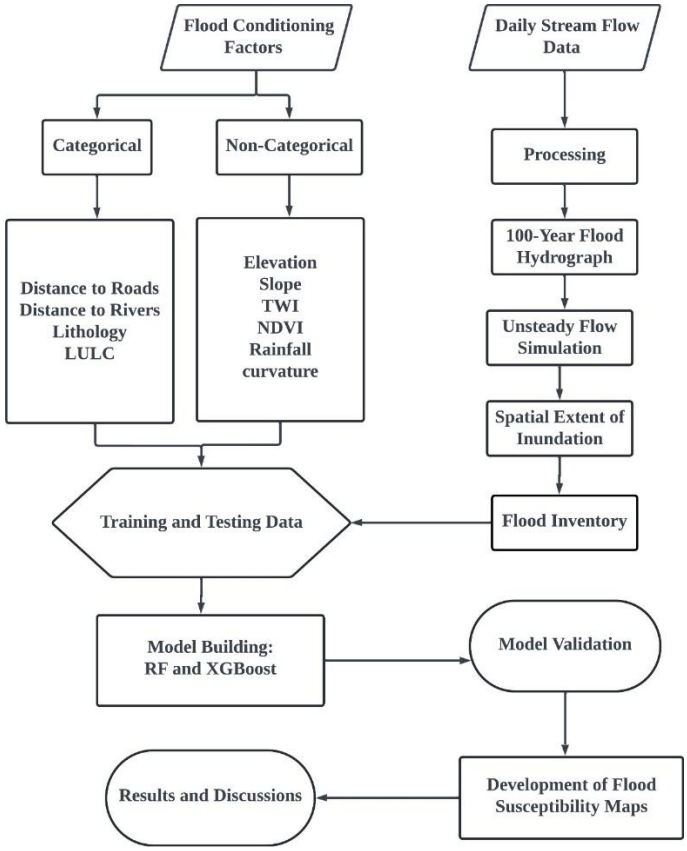

Figure 4. Flowchart of FSM

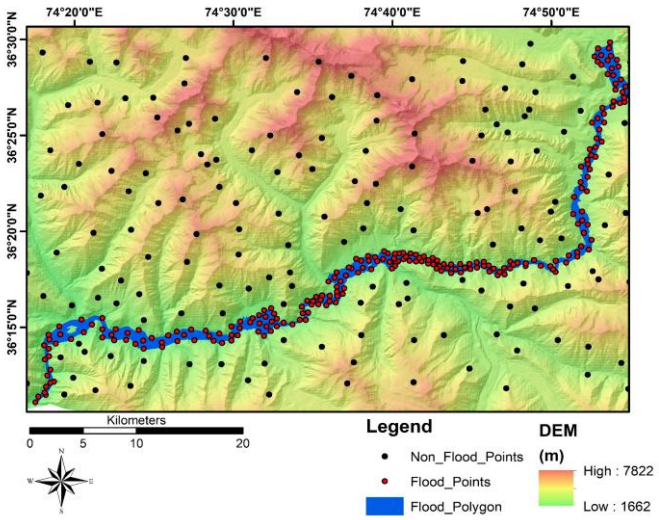

Figure 5. Flood inventory for 100-year flood.

2.3.2. Flood Conditioning Factors

Flood susceptibility is influenced by various factors. Low elevations and gentle slopes promote water accumulation, increasing flood risks, while concave surfaces further concentrate water flow. Areas with higher topographic wetness index (TWI) values and sparse vegetation, as indicated by low NDVI, are more prone to flooding due to reduced infiltration and increased runoff. Urban land cover with impervious surfaces exacerbates flood risks compared to vegetated areas that aid infiltration. Intense rainfall, impermeable

lithology, proximity to rivers, and roads disrupting natural drainage patterns further elevate flood susceptibility in vulnerable regions. These factors are shown in Fig.3.

2.3.3. Random Forest (FR)

RF is a widely used ensemble learning method, well-suited for multi-classification and prediction tasks. It builds a collection of independent decision tree models, each trained on a random subset of data generated through bootstrapping [24]. The general framework for RF is shown in Figure 10. RF is effective for classification problems, as demonstrated in previous studies [25]. Its advantages include insensitivity to multicollinearity, stability with missing or imbalanced data, and reduced overfitting through averaging predictions from multiple decision trees.

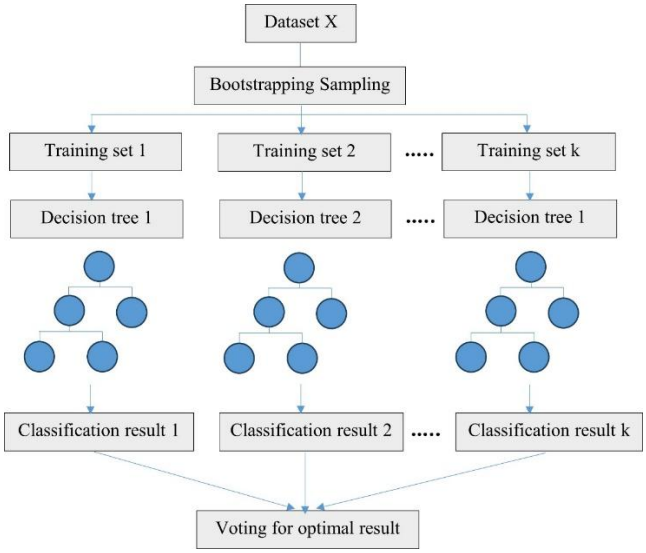

Figure 6. Framework for RF model

2.4. Multi-Hazard Susceptibility Assessment

To generate the Multi-Hazard Susceptibility Map (MHSM), individual susceptibility maps for LSM and FSM are integrated. The methodology for developing LSM varies depending on the geological, geomorphological, and climatic conditions specific to each study area. In the case of the Hunza-Nagar region, the FR model is selected for LSM, while the RF model is chosen for FSM. The overall methodological framework for creating the MHSM is illustrated in Fig 7.

2.4.1. Combine Sum Method

The Combine tool in ArcGIS integrates multiple input rasters by assigning a new value to each unique combination of input values in the resulting output raster. The original cell values from each input raster are preserved in the attribute table of the output raster, with field names corresponding to the input rasters. These fields reflect the unique value combinations from the inputs that generate the output values. In this study, the LSM generated using the FR model and the FSM by RF model are combined using the spatial analyst tool in ArcGIS. Each input raster layer is categorized into five classes—very low, low, moderate, high, and very high—with corresponding numerical values ranging from 1 to 5. The combination of values from the LSM and FSM resulted in 25 unique combinations in the output raster, forming the Multi-Hazard Susceptibility Map (MHSM). This MHSM is then classified into four zones: No Hazard, Landslide, Flood, and Flood+Landslide, based on the unique combinations detailed in Table 1. To obtain the area for each hazard class the MHSM is dissolved by using its 'Hazard Class' as input attribute column in ArcGIS.

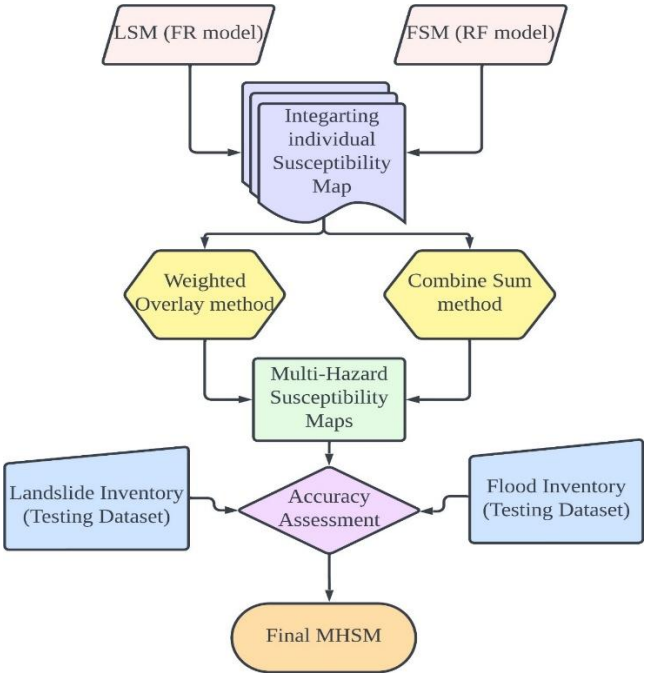

225

Figure 7. Methodology framework for MHSM 226

Table 1. Categorization of the unique combinations of LSM and FSM 227

FSM Raster	LSM Raster	Hazard Class
1	3	No Hazard
1	1	No Hazard
1	2	No Hazard
1	4	Landslide
1	5	Landslide
2	1	No Hazard
2	2	No Hazard
2	3	No Hazard
2	4	Landslide
2	5	Landslide
3	1	No Hazard
3	2	No Hazard
3	3	No Hazard
3	4	Landslide
3	5	Landslide
4	1	Flood
4	2	Flood
4	3	Flood
4	4	Flood+Landslide
4	5	Flood+Landslide
5	3	Flood
5	4	Flood+Landslide
5	5	Flood+Landslide
5	2	Flood
5	1	Flood

Susceptibility Classes: Very Low = 1, Low = 2, Moderate = 3, High = 4, Very High = 5

3. Results and Discussions

3.1. Landslide Susceptibility Assessment

3.1.1. Influence of Causative Factors on Landslides Occurrences

The FR model was employed to assess the spatial influence of various causative factors on landslide occurrences. This model identifies significant relationships between conditioning factors and landslide events, emphasizing their contribution to susceptibility. Among these factors, elevation plays a notable role, with landslides becoming more frequent at higher altitudes. Slope angle is another critical factor, as steeper slopes demonstrate a stronger correlation with landslide events. Curvature of slopes, particularly concave and convex forms, shows a positive association with landslides, whereas flat slopes exhibit a negative relationship. The aspect of slopes also influences landslide susceptibility, with certain orientations being more prone to instability. LULC types such as bare land and built-up areas display a strong connection to landslide occurrences, whereas natural vegetation and snow-covered areas show limited influence. Rainfall is a well-established trigger, with higher rainfall intensities directly increasing landslide susceptibility. Lithology, particularly specific geological formations and their proximity to tectonic features, demonstrates a strong influence on landslide occurrences. Proximity to infrastructure like roads and rivers is also significant, with areas closer to these features showing a higher likelihood of landslides. Lastly, distance to fault lines highlights the impact of tectonic activity on slope stability, with regions near faults being particularly susceptible. Table 2 shows the weightage of each class of conditioning factor for FR model.

Table 2. FR weightages for the classes of each causative factor

Causative Factors	Classes	Class Pixels	% Class pixels	Landslides pixels	% Landslide pixels	FR
Elevation (m)	1662-3353	4663719	25	27530	16	0.64
	3354-4223	6529206	35	41295	24	0.69
	4224-4923	4104073	22	53339	31	1.41
	4924-5648	2425134	13	32692	19	1.46
	5649-7822	932744	5	17206	10	2.00
Slope (Degree)	0-15	373098	2	0	5	0.00
	16-28	1865488	10	10324	11	1.10
	29-39	9327438	50	67104	39	0.78
	40-51	4663719	25	60222	35	1.40
	52-83	2425134	13	25809	15	1.15
Curvature	Concave	4663719	25	87752	51	2.04
	Flat	8394694	45	17206	10	0.22
	Convex	5596463	30	67104	39	1.30
Aspect (Degree)	Flat (-1)	932744	5	0	0	0.00
	North (0-22.5)	2052036	11	18927	11	1.00
	Northeast (22.5-67.5)	2425134	13	15486	9	0.69
	East (67.5-112.5)	2798231	15	18927	11	0.73
	Southeast (112.5-157.5)	1305841	7	25809	15	2.14
	South (157.5-202.5)	2238585	12	22368	13	1.08
	Southwest (202.5-247.5)	1492390	8	20647	12	1.50

	West (247.5-292.5)	1865488	10	27530	16	1.60
	Northwest (292.5337.5)	1678939	9	13765	8	0.89
	North (337.5-360)	1865488	10	8603	5	0.50
LULC	Barelands	4663719	25	80869	47	1.88
	Built area	1119293	6	17206	10	1.67
	Crops	2798231	15	39574	23	1.53
	Flooded Vegetation	373098	2	0	0	0.00
	Glaciers	7088853	38	15486	9	0.24
	Rangeland	186549	1	0	0	0.00
	Trees	1492390	8	6882	4	0.50
	Waterbodies	932744	5	12044	7	1.40
Rainfall (mm)	176-205	1865488	10	12044	7	0.70
	206-224	2798231	15	17206	10	0.67
	225-239	3544426	19	30971	18	0.95
	240-253	4850268	26	46457	27	1.04
	254-280	5596463	30	65384	38	1.27
Lithology	(Jms)	932744	5	5162	3	0.60
	Ks	746195	4	10324	6	1.50
	Mi	1119293	6	18927	11	1.83
	MzPz	559646	3	8603	5	1.67
	Pz	5409914	29	37854	22	0.76
	Pzl	3917524	21	41295	24	1.14
	Q	932744	5	13765	8	1.60
	Ti	3357878	18	18927	11	0.61
	TrCs	373098	2	1721	1	0.50
	Trms	559646	3	12044	7	2.33
	pC	746195	4	3441	2	0.50
Distance-to-Roads (m)	<100	1119293	6	63663	37	6.17
	100-500	1492390	8	34412	20	2.50
	500-1200	1678939	9	25809	15	1.67
	1200-1700	932744	5	18927	11	2.20
	1700-2000	746195	4	10324	6	1.50
	>2000	12685315	68	18927	11	0.16
Distance-to-River (m)	<100	1305841	7	34412	20	2.86
	100-200	559646	3	17206	10	3.33
	200-500	932744	5	25809	15	3.00
	500-700	1865488	10	18927	11	1.10
	700-1000	1678939	9	29251	17	1.89
	>1000	12312218	66	46457	27	0.41
Distance-to-Fault lines (m)	<1000	1865488	10	43016	25	2.50
	1000-2000	2238585	12	20647	12	1.00
	2000-3000	1492390	8	34412	20	2.50
	3000-4000	2052036	11	18927	11	1.00
	4000-5000	1678939	9	25809	15	1.67
	>5000	9327438	50	29251	17	0.34

3.1.2. Landslide susceptibility map

This study employed FR for developing LSM as illustrated in Figure 8. The resulting LSM is classified into five susceptibility classes using a categorical scale as: very low, low, moderate, high, and very high. Geographic Information Systems (GIS) software offers various classification techniques, including standard deviation, natural breaks (Jenk's), manual, equal interval, and quantile methods. The choice of technique depends on the specific data distribution and type. In this study, Jenk's natural breaks classification is applied. This method effectively classifies susceptibility maps based on inherent data value similarities, ensuring effective representation of the spatial distribution of landslide susceptibility. Table 3 details the area covered by each susceptibility zone both in km2 and percentages.

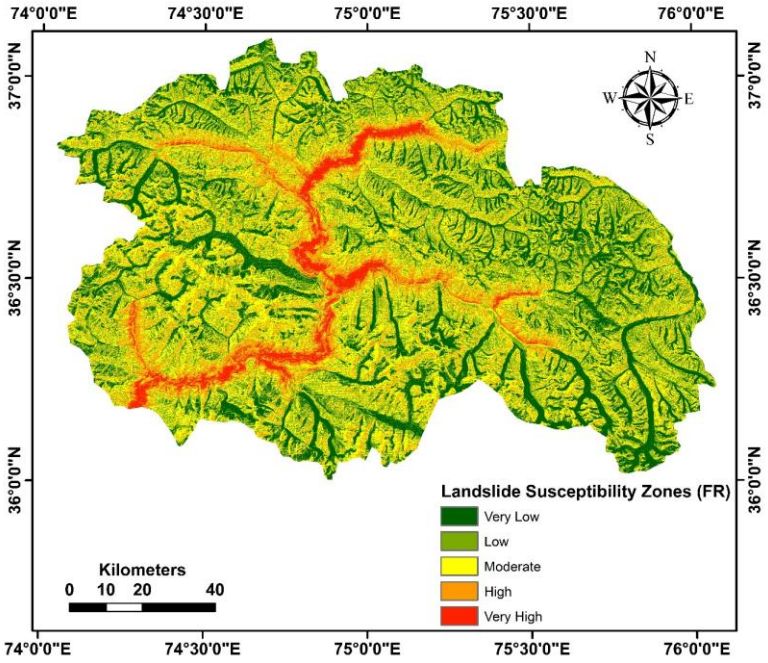

Figure 8. LSM for FR model

Table 1. Area under each susceptibility zone

Susceptibility Zones	Frequency Ratio	
	Area (km²)	% Area
Very Low	3068.22	21.23
Low	4051.96	28.04
Moderate	4937.41	34.17
High	1935.15	13.39
Very High	456.21	3.16
Total	14449	100

3.2. Flood Susceptibility Assessment

3.2.1. Relative Importance of Conditioning Factors for FSMs Development

Tree-based ensemble models offer a significant advantage by considering the interactive effects among independent variables and ranking their relative importance in the modeling process [26]. In this study, four conditioning factors; LULC, distance to roads, distance to rivers, and lithology are categorical variables, while the remaining six factors

are numerical. Each class of categorical variable is treated as a separate input, as a result a total of 37 input layers are fed into the modelling process as independent variables. To enhance model efficiency, variables with negligible influence on flood susceptibility are dropped from the analysis for establishing the final output. The importance of each retained conditioning factor is determined and is visualized in Fig.10.

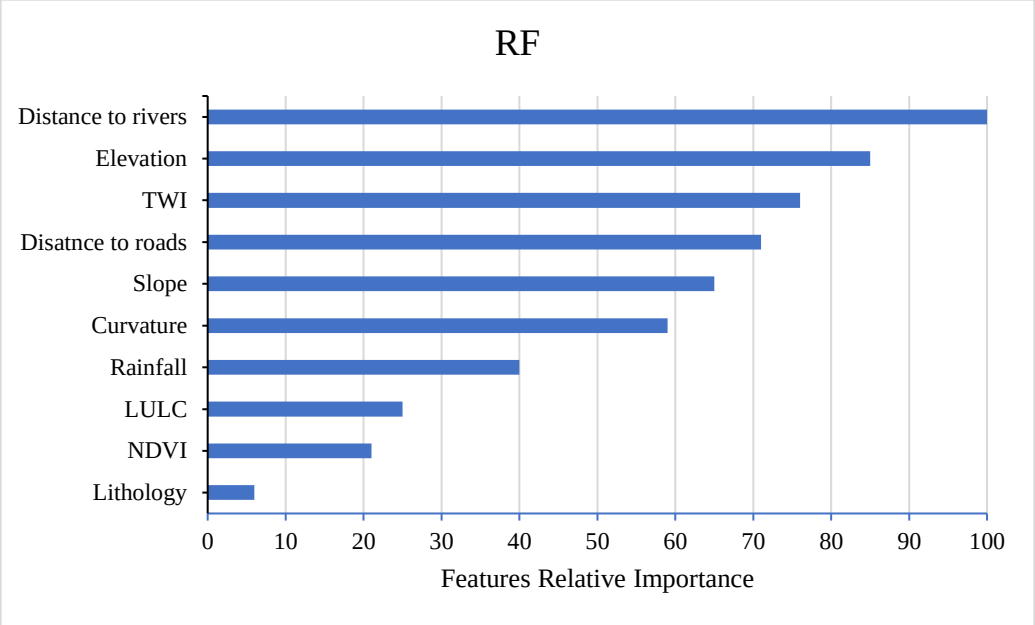

Figure 9. Relative importance of conditioning factors for RF

3.2.2. Development of FSM

Flood susceptibility maps is generated for RF t model which displayed a continuous probability scale ranging from 0 (lowest susceptibility) to 1 (highest susceptibility). To enhance interpretability, the maps are further classified into five categories using the natural breaks method. It's important to note that the specific probability ranges for each category varied between the two models. Each category is assigned a categorical label (very low, low, moderate, high, very high) for improved communication. Fig.10 illustrates both numerical and categorical representations of flood susceptibility. Analysis of the map areas reveals that the highest and lowest susceptibility classes accounted for 4.78% and 50.13% of the total area for the RF model, respectively.

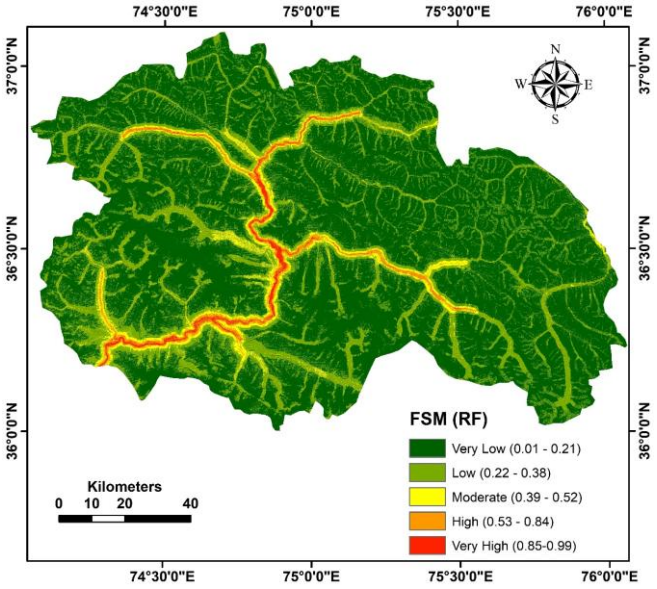

Figure 10. FSM for RF model

3.3. Multi-Hazard Susceptibility Assessment

3.3.1. Development of MHSM

MHSM is generated using the combining sum approach, integrating the LSM from the FR model and the FSM from the RF model. This map is categorized into four hazard types: No Hazard, Flood, Landslide, and Flood+Landslide as shown in Fig. 11. The "No Hazard" zone encompasses an area of 11,952.70 km², while the hazard zones together cover 2,496.23 km². Within the hazard zones, floods occupy an area of 104.87 km², landslides cover 2,079.83 km², and areas affected by both landslides and floods span 311.52 km².

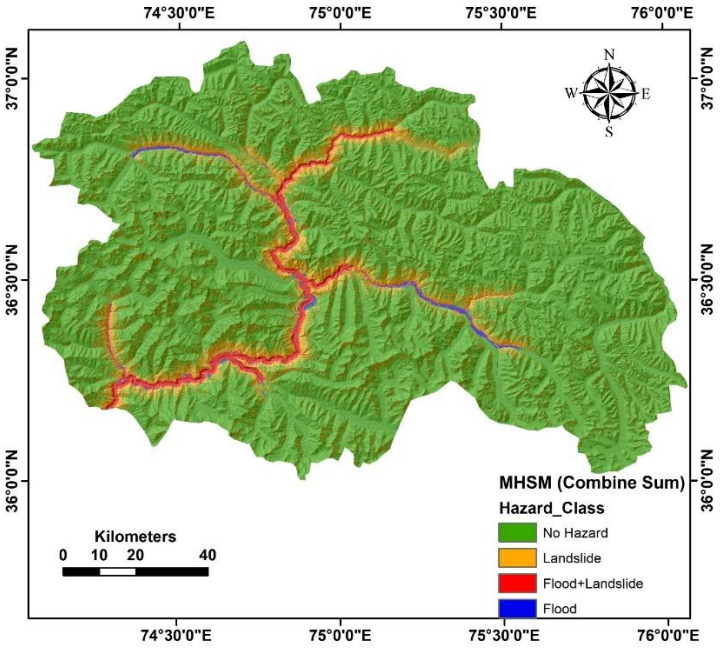

Figure 11. Multi-Hazard susceptibility map for study area

3.4. Accuracy Assessment

The Area Under the Curve-Receiver Operating Characteristic (AUC-ROC) is a key metric for evaluating the accuracy susceptibility models. This method uses 30% dataset for validation and generates an ROC curve, a 2D graph where the vertical axis represents the true positive rate (sensitivity) and the horizontal axis shows the false positive rate (1-specificity). By varying cut-off values, the ROC curve provides a numerical assessment of the model's predictive accuracy. The AUC, ranging from 0.5 to 1, quantifies model precision. An AUC of 1 indicates perfect prediction, while 0.5 represents a model with no discriminatory power. A larger AUC reflects the model's effectiveness in distinguishing landslide-prone areas from non-landslide zones. Both models showed reliable accuracy values. FR model showed an accuracy of 91.6% and RF model 91.2%. These accuracy metrics remained consist for MHSM also which means that the integration of individual susceptibility map does not compromise on accuracy.

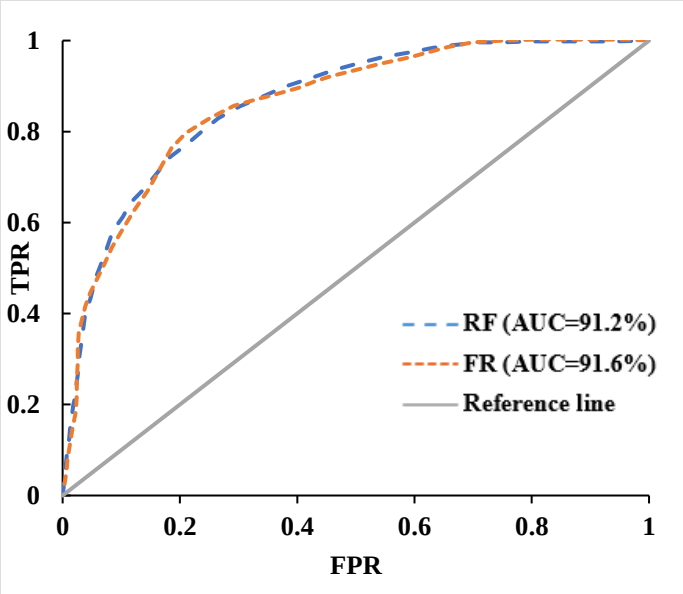

Figure 12. Accuracy assessment plot for FR and RF models.

4. Conclusions

This research presents a comprehensive study on multi-hazard susceptibility mapping (MHSM) for the Hunza-Nagar region in Northern Pakistan, a high-risk area for natural hazards such as landslides and floods. The study integrates statistical and ensemble machine learning models to develop a detailed MHSM, combining the Frequency Ratio (FR) model for landslide susceptibility and the Random Forest (RF) model for flood susceptibility. The combined sum approach effectively represents the region's multi-hazard susceptibility. The findings significantly enhance disaster risk management by providing a detailed visualization of vulnerable areas, aiding land-use planning, infrastructure development, and emergency preparedness. The study introduces an innovative integrated inventory for assessing multiple hazards, which, while yet unvalidated, could streamline hazard assessment processes. Future research is suggested to evaluate its feasibility and reliability. The study highlights limitations, such as static environmental assumptions, and recommends incorporating real-time data to assess multi-hazard susceptibility under climate variability. Expanding the scope to include other hazards like glacial lake outburst floods (GLOFs) and seismic activities would further improve risk assessment. This research work provides a framework for effective multi-hazard susceptibility assessments, promoting targeted disaster risk management strategies to safeguard vulnerable communities in Hunza-Nagar and beyond.

Conflicts of Interest: The authors declare no conflicts of interest.

References

1. J. Chai and H.-Z. Wu, "Prevention/mitigation of natural disasters in urban areas," *Smart Constr. Sustain. Cities*, vol. 1, no. 1, p. 4, 2023.
2. T. R. Linkha, "Landslide and flood disaster: Causes and its responses," *J. Popul. Dev.*, vol. 5, no. 1, pp. 188–202, 2024.
3. K. Abbass, M. Z. Qasim, H. Song, M. Murshed, H. Mahmood, and I. Younis, "A review of the global climate change impacts, adaptation, and sustainable mitigation measures," *Environ. Sci. Pollut. Res.*, vol. 29, no. 28, pp. 42539–42559, 2022.
4. B. Adu-Gyamfi, H. Zuquan, N. Yamazawa, A. Kato, and R. Shaw, "Reflections on science, technology and innovation on the aspirations of the Sendai framework for disaster risk reduction," *Int. J. disaster Resil. built Environ.*, vol. 15, no. 2, pp. 289–302, 2024.
5. R. Shaw and K. Kishore, "Disaster risk reduction and G20: A major step forward," *Prog. Disaster Sci.*, vol. 17, p. 100274, 2023.
6. K. Barquet, M. Englund, K. Inga, K. André, and L. Segnestam, "Conceptualising multiple hazards and cascading effects on critical infrastructures," *Disasters*, vol. 48, no. 1, p. e12591, 2024.
7. M. W. Yaseen, M. Awais, K. Riaz, M. B. Rasheed, M. Waqar, and S. Rasheed, "Artificial Intelligence Based Flood Forecasting for River Hunza at Danyor Station in Pakistan," *Arch. Hydroengineering Environ. Mech.*, vol. 69, no. 1, pp. 59–77, 2022, doi: 10.2478/heem-2022-0005.
8. A. Hussain *et al.*, "Glacier lake outburst flood modeling of Khurdopin glacier lake using HEC-RAS and GIS," in *Селевые потоки: катастрофы, риск, прогноз, защита*, 2020, pp. 208–220.
9. W. Anwar, D. Karim, U. Wahab, K. Din, and D. R. Gurung, "Badswat glacial lake outburst flood and debris dammed lake: a case study," in *Селевые потоки: катастрофы, риск, прогноз, защита*, 2020, pp. 146–156.
10. H. Singh *et al.*, "Assessment of potential present and future glacial lake outburst flood hazard in the Hunza valley: A case study of Shisper and Mochowar glacier," *Sci. Total Environ.*, vol. 868, p. 161717, 2023.
11. V. Sandoval, M. Voss, V. Flörchinger, S. Lorenz, and P. Jafari, "Integrated disaster risk management (IDRM): elements to advance its study and assessment," *Int. J. Disaster Risk Sci.*, vol. 14, no. 3, pp. 343–356, 2023.
12. M. Mondal *et al.*, "Climate change, multi-hazards and society: An empirical study on the coastal community of Indian Sundarban," *Nat. Hazards Res.*, vol. 2, no. 2, pp. 84–96, 2022.
13. D. Kirschbaum *et al.*, "The state of remote sensing capabilities of cascading hazards over High Mountain Asia," *Front. Earth Sci.*, vol. 7, p. 197, 2019.
14. N. Casagli, E. Intrieri, V. Tofani, G. Gigli, and F. Raspini, "Landslide detection, monitoring and prediction with remote-sensing techniques," *Nat. Rev. Earth Environ.*, vol. 4, no. 1, pp. 51–64, 2023.
15. A. L. van Natijne, R. C. Lindenbergh, and T. A. Bogaard, "Machine learning: new potential for local and regional deep-seated landslide nowcasting," *Sensors*, vol. 20, no. 5, p. 1425, 2020.
16. M. Aslam, R. Hayat, N. Pari, A. Sameen, and M. Ahmed, "Climate Change, Flash Floods and Its Consequences: A Case Study of Gilgit-Baltistan," in *Disaster Risk Reduction in Agriculture*, Springer, 2023, pp. 293–310.
17. C. Zhong *et al.*, "Landslide mapping with remote sensing: Challenges and opportunities," *Int. J. Remote Sens.*, vol. 41, no. 4, pp. 1555–1581, 2020.
18. S. Afsar, N. Abbas, and B. Jan, "Comparative study of temperature and rainfall fluctuation in Hunza-nagar District," *J. Basic Appl. Sci.*, vol. 9, pp. 151–156, 2013.
19. S. Ali, P. Biermanns, R. Haider, and K. Reicherter, "Landslide susceptibility mapping by using a geographic information system (GIS) along the China–Pakistan Economic Corridor (Karakoram Highway), Pakistan," *Nat. Hazards Earth Syst. Sci.*, vol. 19, no. 5, pp. 999–1022, 2019.
20. C. Calligaris, C. Michele, T. Shahina, and K. Hawas, "Attabad landslide on 4th January 2010: A pakistani disaster," in *Abstract book*, ISPRA, 2011, p. 614.
21. T. Hayat, H. P. Shah, M. U. Qureshi, and S. Karamat, "Attabad Landslide - Dam disaster in Pakistan 2010 ISSMGE Bulletin : Volume 4 , Issue 3 Case History Attabad Landslide- Dam Disaster in Pakistan 2010," no. December 2015, pp. 20–31, 2010.
22. A. Saha, S. Mandal, and S. Saha, "Geo-spatial approach-based landslide susceptibility mapping using analytical hierarchical process, frequency ratio, logistic regression and their ensemble methods," *SN Appl. Sci.*, vol. 2, no. 10, p. 1647, 2020.
23. B. Youssef *et al.*, "The contribution of the frequency ratio model and the prediction rate for the analysis of landslide risk in the Tizi N'tichka area on the national road (RN9) linking Marrakech and Ouarzazate," *Catena*, vol. 232, p. 107464, 2023.

24. E. Izquierdo-Verdiguier and R. Zurita-Milla, "An evaluation of Guided Regularized Random Forest for classification and regression tasks in remote sensing," *Int. J. Appl. Earth Obs. Geoinf.*, vol. 88, p. 102051, 2020.
25. P. Kulithalai Shiyam Sundar and S. Kundapura, "Spatial mapping of flood susceptibility using decision tree–based machine learning models for the Vembanad Lake System in Kerala, India," *J. Water Resour. Plan. Manag.*, vol. 149, no. 10, p. 4023052, 2023.
26. V. V Mišić, "Optimization of tree ensembles," *Oper. Res.*, vol. 68, no. 5, pp. 1605–1624, 2020.